Topology Optimization with Manufacturable Multi-Material Primitives

by

Oluwanifemi O. Ajayi

B.S. Civil Engineering,
Georgia Institute of Technology, 2018

SUBMITTED TO THE DEPARTMENT OF CIVIL AND ENVIRONMENTAL ENGINEERING IN PARTIAL FULFILLMENT OF THE REQUIREMENTS FOR THE DEGREE OF

MASTER OF ENGINEERING IN CIVIL AND ENVIRONMENTAL ENGINEERING
AT THE
MASSACHUSETTS INSTITUTE OF TECHNOLOGY

June 2019

Signature redacted

Signature of Author: _____
Department of Civil and Environmental Engineering
May 10, 2019

Signature redacted

Certified by: _____
Josephine Voigt Carstensen
Lecturer, Civil and Environmental Engineering and Architecture
Thesis Supervisor

Signature redacted

Accepted by: _____
Heidi Nepf
Donald and Martha Harleman Professor of Civil and Environmental Engineering
Chair, Graduate Program Committee

Topology Optimization with Manufacturable Multi-Material Primitives

by

Oluwanifemi Ajayi

Submitted to the Department of Civil and Environmental Engineering
on May 10, 2019 in Partial Fulfillment of the
Requirements for the Degree of Master of Engineering in
Civil and Environmental Engineering

ABSTRACT

Topology optimization is a field extending to the built environment. Traditionally, optimization focuses mainly on monolithic structures but recently, developments have been made toward determining algorithms for multi-material optimization. A preexisting algorithm is modified to broaden the type of design possible with the method. The algorithm uses a three-phase design problem, a void phase and two other materials, and implements Heaviside Projection Method (HPM) and Rational Approximation of Material Properties (RAMP) method and employs the Method of Moving Asymptotes (MMA) as the gradient based optimizer. Three distinct object projection shapes are proposed, a horizontal, a vertical and a diagonal. The horizontal shaped inclusion enables designs such as, longitudinal reinforced concrete beam design of variable length bars. The vertical shaped inclusion enables designs of columns. The diagonal shaped inclusion allows for design of rebar within more slanted sections of optimized topology. The proposed algorithm is tested on two examples, the cantilever beam and the MBB beam, showing that it works as expected.

Thesis Supervisor: Josephine Voigt Carstensen
Title: Lecturer, Civil and Environmental Engineering and Architecture

Table of Contents

List of Figures

List of Tables

Introduction

Bendsøe and Sigmund [1] describe topology optimization as finding an optimum layout of structure by determining the features, such as element connectivity or number and shape of holes, of solid structure in a domain. It is a design approach that uses mathematical algorithms and computational methods to determine the best possible design in a domain subjected to constraints. It allows engineers to develop innovative designs because it does not require an initial guess from the designer. Topology optimization is a growing field currently being extended to the built environment. Examples include Stromberg et al. [2], that used topology optimization to design high-rise exoskeleton diagrids. Dombernowsky and Søndergaard [3] have also used topology optimization in the design of a reinforced concrete frame, and Jewett and Carstensen [4] discuss the design and constructability of topology-optimized concrete beams.

The recent interest in optimizing construction elements and larger civil structures stems from the goal of decreasing the amount of material used to build infrastructure in the world today. The built environment is said to be a major cause of various environmental problems, including excessive consumption of global resources and pollution from construction as well as material production [5]. According to González and Navarro [6], the construction industry is responsible for almost 50% of energy costs in developed countries. The material volume used in building construction needs to be reduced due to the amount of emissions that buildings are currently approximated to release. De Wolf [7] outlines the impact that structures have on the environment, specifically in term of emissions, and how this knowledge should improve the current approach to the design of buildings.

While topology optimization is an excellent tool being used to achieve the previously stated goal, it is currently most focused on monolithic, single material, structures. Few existing algorithms account for the vast array of multi-material structures, like reinforced concrete beams or fiber-reinforced composites, used in construction. Multi-material topology optimization has been proposed [8,9] and methods to implement the discrete nature of such structures within the design framework have been developed [10,11]. Koh and Guest [10] worked toward this extension of traditional structural topology optimization to multi-material structures by considering implementation of discrete object projection (DOP) using prescribed fixed shape circular primitives as structural inclusions. A primitive here refers to a unit of the discrete object. In the case of a circular primitive, this consists of the discrete object itself enclosed in the

secondary material that determines the spacing between objects. For example, this could be the cross-section of a reinforced concrete beam with the circular discrete objects as the circular reinforcement bars and the minimum spacing between objects defined by the required rebar spacing used in practice. In this case, the algorithm proposed by Koh and Guest [10] would allow simultaneous design of the concrete shape and the rebar placement within the section.

The purpose of this thesis is to develop an algorithm that will add some more complexity to the framework proposed by Koh and Guest [10] by changing the prescribed shape and orientation of the previously circular primitives. The idea is to allow variation in shapes proposed for the primitives to aid the development of more constructible topology-optimized solutions. The algorithm aims to produce continuous elements of stiffer material and varying length embedded within the optimized structure instead of the prespecified inclusion shapes as in the results previously obtained [10]. The algorithm proposed in this thesis thus allows for design of long discrete objects of varying lengths which for instance can be beneficial in the design of longitudinal rebars.

The remainder of this thesis is organized as follows: A literature review is given, showing the context and motivation behind this work and the methodology section discusses the mathematical models used to generate the algorithm. This section is further divided into problem formulation, objective function calculations and sensitivity analysis. The proposed framework is demonstrated on the topology optimization benchmark problems of a cantilever and a simply supported beam and the obtained results are discussed. The final section discusses the benefits of this approach and potential areas for future extensions.

Literature Review

Structural optimization, the process of making an assembly of material carry load in the best way [12], is not a new concept. Through past experience and intuition, the trabeated architecture of ancient Greek temples consisted of beams with members as long as they could be and cross-sections largest at midspan [13] indicating an understanding of structural efficiency. Similarly, in the design of the Pantheon, the use of lighter weight concrete as it approaches the points of least stress [13] shows its designer was thinking of ways to place material only where it was needed. The use of formal optimization, which involves the use of mathematical models to predict optimal conditions based on some criteria that must be satisfied, is a more recent

development. Formal optimization presents itself in a few different ways. One of theses is size optimization [1] which consists of finding the best size for elements within a domain of preset connectivity, that is the arrangement of the structure is predetermined and only the local element sizes have the potential to be changes. Another is shape optimization [1] where the elements of a structure have a predetermined size but the final placement of those elements within the domain is allowed to change. An issue associated with the shape or size optimization is the need for a good initial guess in one aspect of the design, whether the shape, the arrangement or the sizes of the elements.

Topology optimization, which involves the simultaneous optimization of shape and size of a structure, is a step toward solving this problem. Within topology optimization, there are two main types, truss topology optimization and continuum optimization. Truss topology optimization refers to optimization of a domain containing a fixed set of nodal points connected by truss elements, creating a ground structure, which have variable cross-sectional area as the design variables [1]. On the other hand, continuum optimization is based on continuum finite element meshing; instead of the truss elements described above, it utilizes small fractions of the whole volume of the domain [1]. Within the density-based approach, the optimal design is determined by assigning a 0 or 1, i.e. void or material, value as the density to each element, where density is the design variable in this method. The common theme in the work done thus far is the homogeneity of the materials used in optimization. As part of the simplification, material properties, such as Young's modulus, of all the elements are typically assumed to be the same, or at least constant within a single element. In reality, many structures are constructed by the combination of material, for instance, reinforced concrete beams, fiber reinforced composites to name a few.

Several researchers have proposed multi-material topology optimization as a means to improve applicability of topology optimized designs in practice. Bendsøe and Sigmund [8] proposed a methodology to implement material interpolation between two or three material structures. Gaynor et al. [9] proposed a hybrid truss-continuum optimization technique to simultaneously optimize the concrete and required tensile steel rebar in reinforced concrete. Zhang et al. [14,15] proposed an algorithm for multi-material optimization of truss structures using the ground structure method and implementing level sets.

In practice, most multi-material structures have a discrete nature associated with one of its phases. Again, an example is reinforced concrete, where the concrete is distinct from the steel reinforcements bars. To ensure that the discrete nature of these structures is accounted for within the algorithm, the discrete object projection method was developed. Guest [16] presents this topic in detail and delivers an algorithm to optimize object layouts within a user defined structure.

As mentioned, Koh and Guest [10] developed an extension that performs topology optimization such that both structure and layout of circular inclusions is designed simultaneously. This paper seeks to extend the work Koh and Guest began. The methodology is taken directly and modified to fit new shapes of desirable discrete objects.

Methodology

Setting up the topology optimization problem takes a few steps. First, the design domain needs to be determined. In the context of topology optimization, that refers to the possible support conditions of the domain, the applied loads, and potential design restrictions, for instance structural weight [1]. Next is to define the problem formulation, including determining the objective function, the specific constraints for the problem and the method of optimization to be utilized. This work discusses the development of an algorithm that optimizes a structure using two materials. As its basis, it uses density-based continuum topology optimization of a structure with compliance as the objective function and material volume as the constraint [17]. A fundamental requirement for any structure, optimized or not, is equilibrium, and as a result, the finite element method will be used to ensure static equilibrium. The typical compliance objective problem formulation used, is given in Eq. (1).

$$\begin{aligned} \underset{\phi}{\text{minimize}} \quad & C = \boldsymbol{F}^T \boldsymbol{d} \\ \textit{subject to} \quad & \boldsymbol{K}(\phi)\boldsymbol{d} = \boldsymbol{F} \\ & \sum_{\forall e \in \Omega} \rho^e(\phi) v^e \leq V_{max} \qquad for\ i = 1, \dots, N \\ & 0 \leq \phi_i \leq \phi_{max} \qquad \forall i \in \Omega \end{aligned} \tag{1}$$

where C is compliance, $\mathbf{F}$ is the global vector of the nodal forces and $\mathbf{d}$ is the global vector of nodal displacements. $\mathbf{K}$ is the global stiffness matrix, ρ^e is the element phase indicator, v^e is the

element volume and V_{max} is the overall structural volume constraint. ϕ_i is the design variable assigned to each element in the domain and ϕ_{max} is the upper bound on the design variables.

Here, ρ^e is the variable that indicates whether an element is void or contains material so it can take only a value of 0 and 1. The stiffness of an element, $\boldsymbol{K}^e$, is determined by multiplying the element stiffness if material is fully present, $\boldsymbol{K}_0^e$, with the density variable, ρ^e. In order to enforce the 0-1 binary, a penalty function is used. Typically, the Solid Isotropic Material with Penalization (SIMP) [18] method or Rational Approximation of Material Properties (RAMP) [23]. Both methods work by making the intermediate densities inefficient causing the optimizer to choose the more efficient densities.

Using a penalty function typically causes the optimizer to produce results with checkerboarding. To avoid checkerboarding, the density variables are filtered [18]. The filtering is done by introducing a different variable, ϕ, which is used as the design variable. ϕ is then filtered to obtain ρ^e. These filters make each element's density dependent on the density of the elements surrounding it thereby preventing elements in the same vicinity from continuously varying between void and full. There are multiple ways of doing filtering, for an in-depth view, see the paper *Topology Optimization approaches* by Sigmund and Maute [19]. The algorithm in this work uses the Heaviside Projection Method (HPM).

The problem formulation, developed by Koh and Guest [10], utilized in this paper is given below in Eq. (2). It is derived from the problem for a typical compliance objective problem as described above in Eq. (1). It combines the DOP optimization method outlined by Guest [16] with the tradition compliance minimization problem. However, to achieve the optimization of the topology while simultaneously optimizing the placement of discrete objects within the structure, the element density ρ^e is defined as the function of two variables, ρ_T^e, describing a topology phase and ρ_D^e, that refers to an inclusion phase. For instance, a reinforced concrete beam, where the "topology" refers to the concrete and the "inclusion" the stiff steel rebars enclosed within it. The variables controlling the topology ρ_T^e are essentially the same as ρ^e in Eq. (1). The discrete object densities ρ_D^e are equal to ρ^e from [16]. Like ρ^e, the set of desired values for ρ_T^e and ρ_D^e is [0,1]. A second volume constraint is added to the problem to give the designer control over the total mass of the discrete objects to be included. The updated problem formulation is given in Eq. (2).

$$\underset{\phi_D,\phi_T}{\text{minimize}} \qquad C = \boldsymbol{F}^T\boldsymbol{d} \tag{2}$$

$$
\begin{aligned}
\textit{subject to} \quad & \boldsymbol{K}(\phi_D, \phi_T)\boldsymbol{d} = \boldsymbol{F} \\
& \sum_{\forall e \in \Omega} \rho_T^e(\phi_T) v^e \leq V_T \qquad for\ i = 1, \dots, N \\
& \sum_{\forall e \in \Omega} \rho_D^e(\phi_D) \rho_T^e(\phi_T) v^e \leq V_S \qquad for\ i = 1, \dots, N \\
& 0 \leq \phi_i \leq \phi_{max} \qquad \forall i \in \Omega
\end{aligned}
$$

where C, $\mathbf{F}$, $\mathbf{d}$, $\mathbf{K}$, v^e, ϕ_i and ϕ_{max} are as described above, ϕ_D, ϕ_T are the inclusion and topology design variables respectively, ρ_T^e is the topology phase variable, ρ_D^e is the inclusion phase variable, V_T is the maximum allowable volume of material in the structure and V_S is the maximum allowable volume of stiff material.

Because of the distinction between topology and inclusion densities, the number of design variables doubles. Now each element has a variable assigned to those aforementioned phases. The densities are determined by filtering the design variables. The filtering is done twice for each element; one for the topology design variables and once for the inclusion design variables. The element density, ρ^e, is determined by combining these two projects using $\rho_T^e(1 + \rho_D^e)/2$. All the steps taken here are the same as the ones taken by Koh and Guest [10] except the inclusion filters are modified to give the algorithm more breath on the kinds of solutions that can be achieved. The following subsections will describe the methods used to calculate the objective function and constraints as well as their sensitivity analyses.

Filtering for Circular Inclusions

The functions showing the inclusion filter function that separates the compliant enclosure from the stiff inclusion are described as follows. These equations were adapted mainly from Koh and Guest [10].

The implementation of designing discrete objects with topology optimization is done by defining two sets. A local set is defined as N_L^e and an enclosure set by N_E^e. The local set is representative of the discrete objects to be inserted in the topology. The enclosure set is necessary to prevent the discrete objects from overlapping and provides the designer with control over the minimum spacing between objects. These sets are shown in Figure 1 and given by Eq. (3).

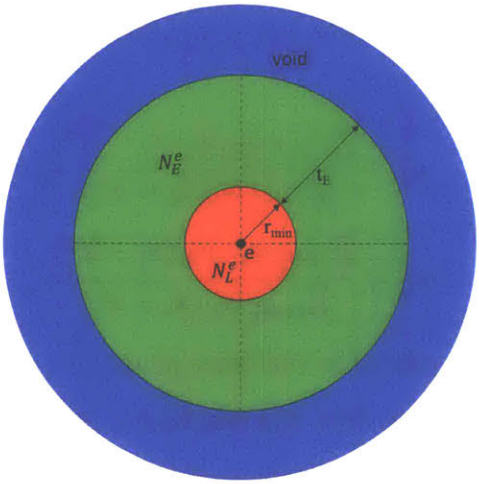

Figure 1. Circular Inclusion Primitive that consists of a circular object (red) of radius r_{min}, an enclosure (green) that controls the minimum object spacing t_E and a void (blue) that is not affected by the element e

$$\begin{aligned} i \in N_L^e \quad if \ \|\boldsymbol{x}_i - \overline{\boldsymbol{x}}^e\| \leq r_{min_D} \\ i \in N_E^e \quad if \ r_{min_D} \leq \|\boldsymbol{x}_i - \overline{\boldsymbol{x}}^e\| \leq r_{min_D} + t_E \end{aligned} \tag{3}$$

where $\boldsymbol{x}_i$ is the location of the design variable in question and $\overline{\boldsymbol{x}}^e$ is the centroid of element e. The combined discrete object element phase, ρ_D^e, can indicate one of two material phases; (i) the enclosure phase that has a compliant material, or (ii) the inclusion phase that has a stiff material. In Fig. 1 the compliant phase is displayed as green and the stiff phase is red. The combined discrete object phase is determined by Eq. (4) [10,11,16].

$$\rho_D^e = \frac{\rho_L^e(2 - \rho_E^e)}{2} \tag{4}$$

where, ρ_L^e indicates the inclusion or local phase and ρ_E^e indicates the enclosure phase. The values of these local and enclosure phases are calculate using the heaviside projection method [20] as shown in (5).

$$\begin{aligned} \rho_L^e &= 1 - e^{-\beta_L \mu_L^e(\phi_D)} + \frac{\mu_L^e(\phi_D)}{\phi_{max}} e^{-\beta_L \phi_{max}} \\ \rho_E^e &= 1 - e^{-\beta_E \mu_E^e(\phi_D)} + \frac{\mu_E^e(\phi_D)}{\phi_{max}} e^{-\beta_E \phi_{max}} \end{aligned} \tag{5}$$

where β_L and β_E are the heaviside exponents for the local and enclosure phases respectively. The density filter is used to find $\mu_L^e(\phi_D)$ and $\mu_E^e(\phi_D)$ that are the filtered design variables [21,22]. It forces an elements final density value to be dependent on the value of the elements surrounding it. Each elements density is therefore determined as a weighted average of the design variables

close to it. The values considered close are determined from the local and enclosure sets described earlier (see Eq. 3).

$$\mu_L^e = \frac{\sum_{i \in N_L^e} \phi_{D,i} w_L(\boldsymbol{x}_i - \bar{\boldsymbol{x}}^e)}{\sum_{i \in N_L^e} w_L(\boldsymbol{x}_i - \bar{\boldsymbol{x}}^e)}$$
$$\mu_E^e = \frac{\sum_{i \in N_E^e} \phi_{D,i} w_E(\boldsymbol{x}_i - \bar{\boldsymbol{x}}^e)}{\sum_{i \in N_E^e} w_E(\boldsymbol{x}_i - \bar{\boldsymbol{x}}^e)} \tag{6}$$

where $\phi_{D,i}$ is the design variable related to enclosure phase, $w_L(\boldsymbol{x}_i - \bar{\boldsymbol{x}}^e)$ and $w_E(\boldsymbol{x}_i - \bar{\boldsymbol{x}}^e)$ are the weights assigned to all design variables as a function of the design variables in question. The set describing the variables of interest per element, N_T^e, is given below, shown in Figure 2 and Eq. (7).

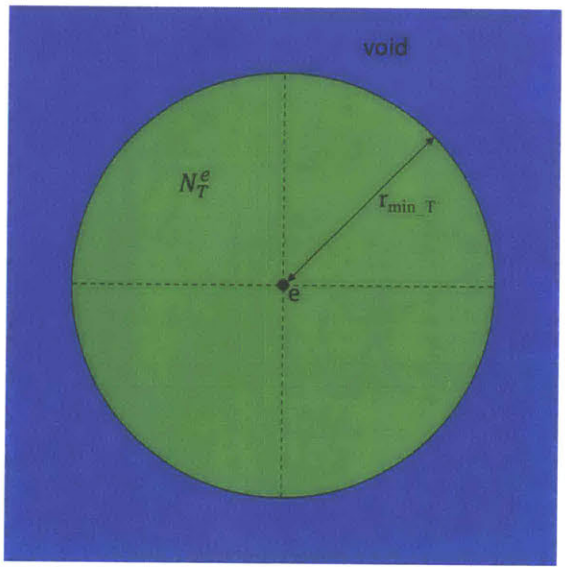

Figure 2. Topology Filter Region consists of a circular region (green) of radius r_{min_T} that controls the minimum length scale of the structure and a void (blue) that is not affected by the element e

$$i \in N_T^e \quad if \ \|\boldsymbol{x}_i - \bar{\boldsymbol{x}}^e\| \leq r_{min_T} \tag{7}$$

where $\boldsymbol{x}_i$ and $\bar{\boldsymbol{x}}^e$ are the same as described above and r_{min_T} is the user defined minimum length scale of the topological feature. It can for example be determined as the smallest sized element manufacturable. The element densities indicating the topology phase, ρ_T^e, is determined using heaviside projection as well:

$$\rho_T^e = 1 - e^{-\beta_T \mu_T^e(\phi_T)} + \frac{\mu_T^e(\phi_T)}{\phi_{max}} e^{-\beta_T \phi_{max}} \tag{8}$$

where β_T is the heaviside exponent relating to the topology. $\mu_T^e(\phi_T)$ is the filtered topology design variable, determined as a weighted average of neighboring elements.

$$\mu_T^e = \frac{\sum_{i \in N_T^e} \phi_{T,i} w_T(\boldsymbol{x}_i - \bar{\boldsymbol{x}}^e)}{\sum_{i \in N_T^e} w_T(\boldsymbol{x}_i - \bar{\boldsymbol{x}}^e)} \tag{9}$$

where $\phi_{T,i}$ is the topology design variable, and $w_T(\boldsymbol{x}_i - \bar{\boldsymbol{x}}^e)$ is the weight assigned to all design variables as a function of the design variables in question. It's given for all phases as described in Eq. (10).

$$w_R(\boldsymbol{x}_i - \bar{\boldsymbol{x}}^e) = \begin{Bmatrix} 1 & if\ \boldsymbol{x}_i \in \Omega_R^i \\ 0 & otherwise \end{Bmatrix} \tag{10}$$

where R can be L, E or T.

The combined stiffness of each element, E^e, is a function of both the inclusion and the topology design variables, ϕ_D and ϕ_D, respectively. It is given by Eq. (11) that uses the multi-material formulation suggested by Bendsøe and Sigmund [8].

$$E^e(\phi_D, \phi_T) = \rho_T^e(\phi_T)(E_1 + \rho_D^e(\phi_D)(E_2 - E_1)) \tag{11}$$

where E_1 and E_2 are the varying young's moduli for the compliant and stiff phases. Where E_1 is the stiffness of the concrete and E_2 is the stiffness of the steel rebar for a reinforced concrete section.

Every element will be assigned on of the three aforementioned phases (void, topology, inclusion) displayed in Figure 1 and Figure 2. The algorithm is defined such that the optimal topology is determined, and then stiffer material is efficiently included within the topology. As a result, the stiff material is prescribed to necessarily fall within the topology. To enforce this, the density function in Eq. (11) always results in 0 if the topology phase, ρ_T^e, is 0.

When an element has no inclusion, i.e. $\rho_D^e = 0$, the element stiffness, E, is E_1, the compliant material stiffness. If an element does have inclusion, i.e. $\rho_D^e = 1$, E resolves to E_2, the stiffness of the stiff material. As determined based on Eq. (4) with values summarized in Table 1 below, ρ_D^e can have a value of 0.5 which indicates a mixed-phase stiff and compliant material. In order to achieve the desired binary, the element stiffness, E^e, is calculated using a penalty function on the topology and inclusion phase variables. The penalty function used in this work is the RAMP method [23]. To prevent matrix singularity and other problems associated with zero value ρ^e, a small number, ρ_{min}^e, is added [24].

$$E^e(\phi_D, \phi_T) = \frac{\rho_T^e(\phi_T)}{1+\eta(1-\rho_T^e(\phi_T))}\left(E_1 + \frac{\rho_D^e(\phi_D)}{1+\eta(1-\rho_D^e(\phi_D))}(E_2 - E_1)\right) + \rho_{min}^e \qquad (12)$$

Table 1. ρ_D^e value summary table for topology optimization of structures with discrete inclusions. Reproduced from Koh and Guest [10]

ρ_L^e	ρ_E^e	ρ_D^e	Material Phase
0	0	0	Compliant
0	1	0	Compliant
1	0	1	Stiff
1	1	0.5	Mixed

To improve efficiency and decrease complexity of the problem, the nested method is adopted. Here, the equilibrium constraint, $\mathbf{Kd} - \mathbf{F} = 0$, is embedded within the compliance function. This means in every iteration, the displacement, $\mathbf{d}$, is calculated as, $\mathbf{K}^{-1}\mathbf{F}$ before multiplying it with the transpose of the force vector to determine the structures compliance. Though optimizing multi-material structures with varying young's moduli, the stiffness matrix is determined first by assigning an arbitrary constant young's modulus to every element and then calculating an initial stiffness, $\boldsymbol{K}_0^e$ [25]. This stiffness is multiplied by the stiffness factor, E^e, determined in Eq. (12) to obtain the element stiffness.

$$\boldsymbol{K}^e = E^e(\phi_D, \phi_T)\boldsymbol{K}_0^e \qquad (13)$$

Sensitivity Analysis

As with any density-based topology optimization problem that is solved using a gradient based optimizer, the sensitivities of the objective function and the constraints are required. The following equations will show how these values are determined for the algorithm described above. Since there are two design variables, the sensitivity of the objective is taken as a partial derivative with respect to both:

$$\frac{\partial C}{\partial \phi_{D,i}} = \sum_{\forall e \in \Omega} \frac{\partial C}{\partial \rho_D^e}\frac{\partial \rho_D^e}{\partial \phi_{D,i}} \qquad \forall i \in \phi_D \qquad (14)$$

$$\frac{\partial C}{\partial \phi_{T,i}} = \sum_{\forall e \in \Omega} \frac{\partial C}{\partial \rho_T^e} \frac{\partial \rho_T^e}{\partial \phi_{T,i}} \qquad \forall i \in \phi_T \tag{15}$$

As shown above, these are determined using the chain rule. The objective function sensitivities can be calculated using the adjoint method [1,12]. The partial derivative of the compliance with respect to the phase densities is given in Eq. (16).

$$\frac{\partial C}{\partial \rho_R^e} = -\boldsymbol{d}^T \frac{\partial \boldsymbol{K}}{\partial \rho_R^e} \boldsymbol{d} \tag{16}$$

where R is D or T. The partial derivative of stiffness with respect to the phase densities is given in Eq. (17).

$$\frac{\partial \boldsymbol{K}}{\partial \rho_R^e} = \frac{\partial E^e}{\partial \rho_R^e} \boldsymbol{K}_0^e \tag{17}$$

The partial derivative of stiffness factor with respect to the phase densities is given in Eq. (18) and are determined by direct differentiation of Eq. (12):

$$\begin{aligned} \frac{\partial E^e}{\partial \rho_T^e} &= \frac{1+\eta}{(1+\eta(1-\rho_T^e))^2}\left(E_1 + \frac{\rho_D^e}{1+\eta(1-\rho_D^e)}(E_2 - E_1)\right) \\ \frac{\partial E^e}{\partial \rho_D^e} &= \frac{\rho_T^e}{1+\eta(1-\rho_T^e)}\left(\frac{1+\eta}{(1+\eta(1-\rho_D^e))^2}(E_2 - E_1)\right) \end{aligned} \tag{18}$$

The sensitivity of the filtered variables with respect to the phase densities is derived using the chain rule and given in Eq. (19)

$$\frac{\partial \rho_D^e}{\partial \phi_{D,i}} = \frac{1}{2}\left((2-\rho_E^e)\frac{\partial \rho_L^e}{\partial \phi_{D,i}} - \rho_L^e \frac{\partial \rho_E^e}{\partial \phi_{D,i}}\right) \tag{19}$$

The partial derivatives of the local and inclusion phase densities are given by differentiating the heaviside projection equations in Eq. (5).

$$\frac{\partial \rho_R^e}{\partial \phi_{D,i}} = \left(\beta_R e^{-\beta_R \mu_R^e(\phi_D)} + \frac{1}{\phi_{max}} e^{-\beta_R \phi_{max}}\right)\frac{\partial \mu_R^e}{\partial \phi_{D,i}} \tag{20}$$

where R is L or E. The sensitivity for the filtered enclosure variables, μ_R^e, using a uniformly weighted function, are $w = 0$ *or* 1, is in Eq. (21).

$$\frac{\partial \mu_R^e}{\partial \phi_{D,i}} = \frac{1}{\sum_{i \in N_R^e} w_R(\boldsymbol{x}_i - \bar{\boldsymbol{x}}^e)} \tag{21}$$

where R is the same as listed above. A similar expression for the topology specific density sensitivities is given in Eq. (22).

$$\frac{\partial \rho_T^e}{\partial \phi_{T,i}} = \left(\beta_T e^{-\beta_T \mu_T^e(\phi_T)} + \frac{1}{\phi_{max}} e^{-\beta_T \phi_{max}}\right) \frac{\partial \mu_T^e}{\partial \phi_{T,i}} \tag{22}$$

Likewise, the inner partial derivative for the filtered topology design variable, μ_T^e, is given in Eq. (23).

$$\frac{\partial \mu_T^e}{\partial \phi_{T,i}} = \frac{1}{\sum_{i \in N_T^e} w_T(\boldsymbol{x}_i - \bar{\boldsymbol{x}}^e)} \tag{23}$$

Optimization Method

This algorithm utilizes the method of moving asymptotes (MMA) as the gradient-based optimizer [26]. The continuation method is used where the RAMP exponent, η, varies from 0 and to 40 and the value of the heaviside exponents, β, varies from 5 to 50. All projections use the same β value. Both variables change over 12 iterations.

Cantilever Beam Design

This test case is a simple cantilever beam with a single gravity load applied on the far end at mid-height. Shown in Figure 3 with length, L, at 40 units, height, H, at 25 units, thickness, t, at 1 unit, and load, P, at 10 units. The finite element mesh used is 160 × 100. The minimum inclusion scale, r_{min_D} is 0.25 units, the minimum distance between objects, t_E, is 0.5 units and the topology length scale, r_{min_T}, is 0.75 units. The maximum volume of material, V_T, is 50% of V, with a maximum inclusion volume, V_S, of 10% of V for the first example and 7.5% for the subsequent ones. The Poisson's ratio, ν, is 0.3, initial Young's modulus, E, is 100 with material young's modulus factors, E_1 and E_2, at 1 and 3 respectively. The design variable upper bound, φ_{max}, is 1.

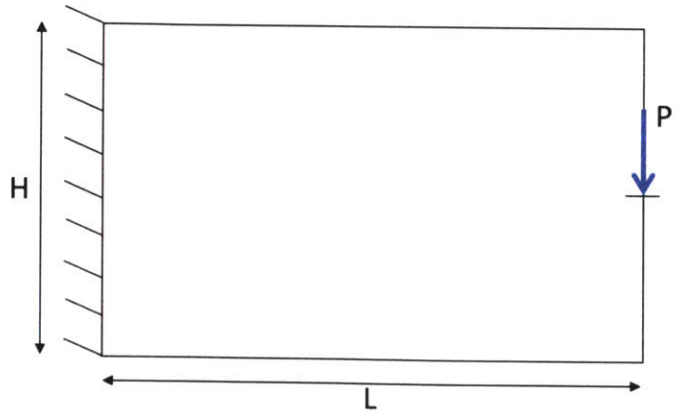

Figure 3. Cantilever Beam Design Domain

Figure 4 shows the solution obtained for the conditions stated above. Based on these results, the replicated algorithm appears to work the same as the original. Toward the areas of higher stress in a cantilever beam, it does have more trouble separating inclusions and hence fulfilling the spacing requirement. This was also observed in the original work [10]. The obtained compliance for the design in Fig. 4 is 32.76.

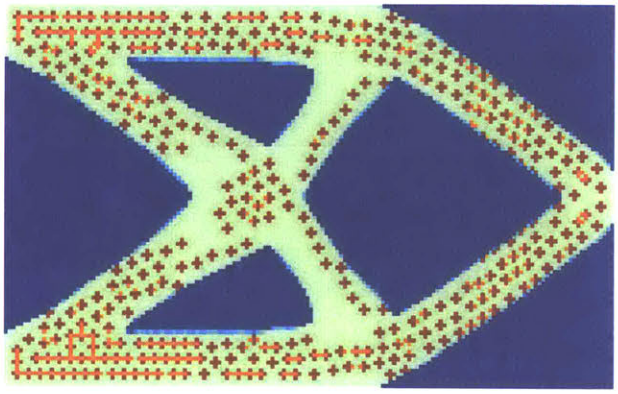

Figure 4. Cantilever Beam with Circular Inclusions at 10% Volume ratio

Figure 5 shows a cantilever design obtained with a smaller inclusion mass allowed. The compliance is not surprisingly increased to 33.76. As expected, the algorithm placed stiff material around the

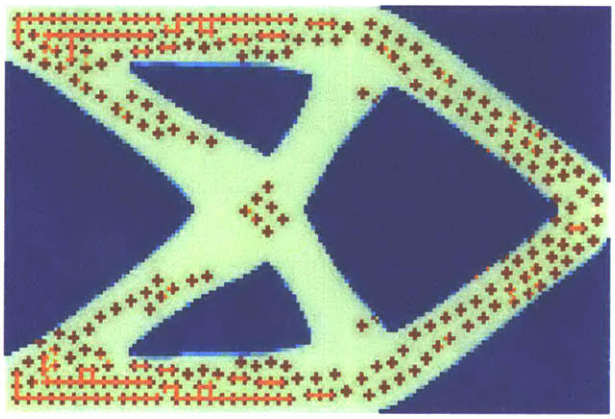

Figure 5. Cantilever Beam with Circular Inclusions at 7.5% Volume ratio

Extending Discrete Object Filters to Allow New Inclusion Shapes

As stated earlier, the purpose of this thesis is to develop an algorithm that allows for long variable length discrete objects using different shape primitives. To achieve this, only the discrete object filter defined in the algorithm needs to change. Three distinct object filters are proposed in this work; horizontal inclusions, vertical inclusions and diagonal inclusions sloped at an 45° angle. The next subsection discusses the changes this prompts to the topology filter. The following three subsections discuss the herein suggested enclosure filters.

Topology Filter

As will be seen in the following sections, the newly proposed inclusion have square outlines. Though the shape outline of all the proposed primitives is square, the topology filter needs to stay circular in order to preserve the smooth curves along the boundary of the topology solution. The topology region is determined as described in Eq. (7) with an added restriction on r_{min_T} given in Eq. (24). This ensures the inclusion geometry fits within the minimum length scale.

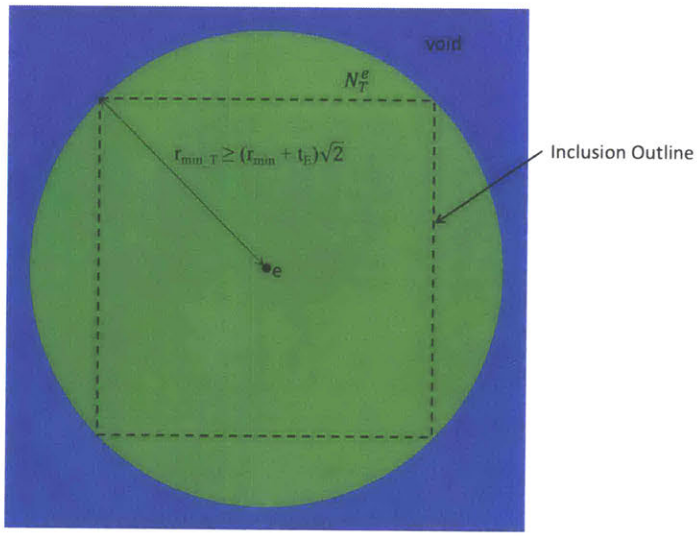

Figure 6. Topology Filter Region consists of a circular region (green) of radius r_{min_T} that controls the minimum length scale of the structure and a void (blue) that is not affected by the element e

$$r_{min_T} \geq (r_{min} + t_E)\sqrt{2} \tag{24}$$

Horizontal Primitives Filter

The herein presented horizontal primitives indented to aid longitudinal beam design. It allows the beams to be designed with long discrete elements of varying length. By freeing up both ends of the enclosure, the discrete objects are allowed to be overlap end-to-end.

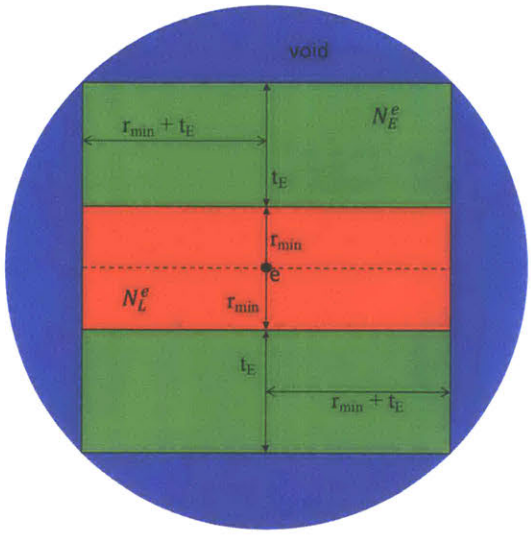

Figure 7. Horizontal Inclusion Primitive consists of a horizontal rectangular object (red) of radius r_{min}, an enclosure (green) that controls the minimum object spacing t_E and a void (blue) that is not affected by the element e as in Figure 1

Figure 7 shows the local and enclosure phases for a new horizontal primitive. The neighborhoods are now determined using Eq. (25).

$$\begin{aligned} i \in N_L^e \quad if \begin{cases} |x_i - \bar{x}^e| \leq r_{min_D} + t_E \\ |y_i - \bar{y}^e| \leq r_{min_D} \end{cases} \\ i \in N_E^e \quad if \begin{cases} |x_i - \bar{x}^e| \leq r_{min_D} + t_E \\ r_{min_D} < |y_i - \bar{y}^e| \leq r_{min_D} + t_E \end{cases} \end{aligned} \tag{25}$$

where x_i and $\bar{x}^e$ are the x-coordinates of the design variable and the element respectively, and y_i and $\bar{y}^e$ are the y-coordinates of the design variable and the element respectively.

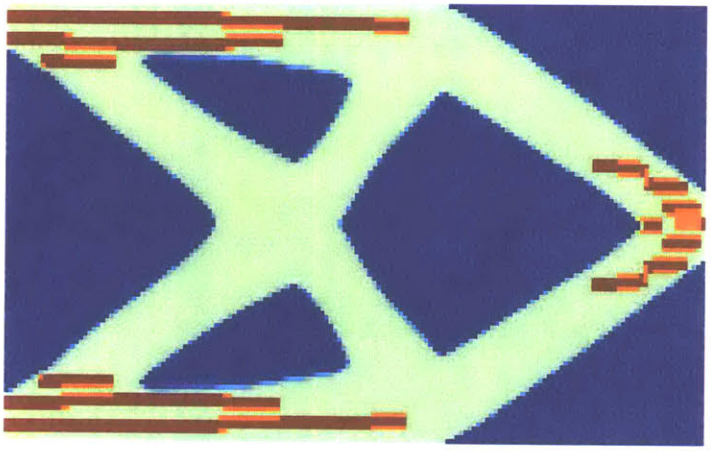

Figure 8. Cantilever Beam with Horizontal Inclusions

In Figure 8, the solution to the cantilever design problem with longitudinal inclusions is displayed. The optimizer places the inclusions in the regions of higher stress in the cantilever beam, around the supports and point load. In this case, compliance decreased drastically to 29.83. This is as a result of the horizontal inclusions placed at the point of highest moment and with the inclusions continuous in the direction reactions are expected.

Vertical Primitive Filter

Some design domains, including column design problems, would need stiff material designed in the vertical direction. Like the horizontal filter, the vertical filter has no compliant material on the top and bottom to allow material to lengthen through the structure.

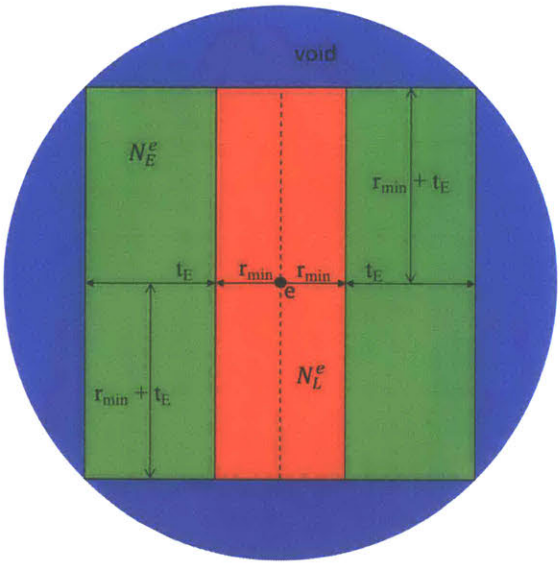

Figure 9. Vertical Inclusion Primitive consists of a vertical rectangular object (red) of radius r_{min}, an enclosure (green) that controls the minimum object spacing t_E and a void (blue) that is not affected by the element e as in Figure 1

The vertical filter, displayed in Figure 9, is determined by interchanging the x and y regions for the intervals determined for the horizontal filter in Figure 7 given in Eq. (26).

$$\begin{aligned} i \in N_L^e \quad if \begin{cases} |x_i - \bar{x}^e| \leq r_{min_D} \\ |y_i - \bar{y}^e| \leq r_{min_D} + t_E \end{cases} \\ i \in N_E^e \quad if \begin{cases} r_{min_D} < |x_i - \bar{x}^e| \leq r_{min_D} + t_E \\ |y_i - \bar{y}^e| \leq r_{min_D} + t_E \end{cases} \end{aligned} \tag{26}$$

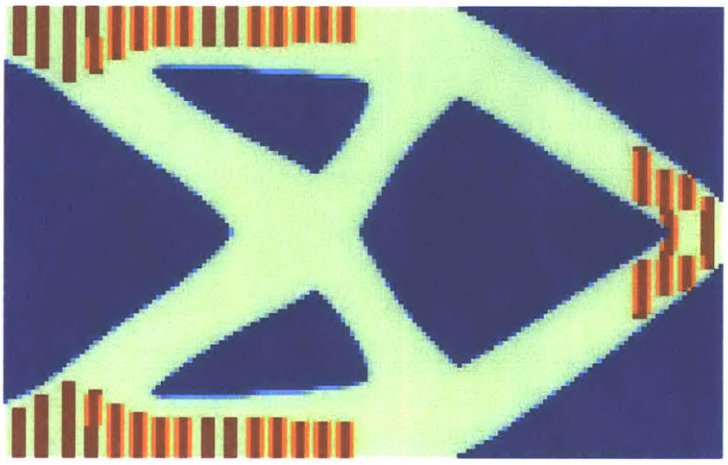

Figure 10. Cantilever Beam with Vertical Inclusions

Figure 10 shows the results obtained from the cantilever beam example described above using vertical filters. The optimizer places material around the load and supports in this case as

well but the compliance remains similar to that of the circular inclusions. The compliance is 33.16 in this case. This is because as the reaction lines, which are horizontal approaching the supports, are continually interrupted by compliant material induced by the minimum spacing between inclusions.

Angled (45º) Primitive Filter

The angled filter is useful because structure may be slanted. Ideally, the inclusions would fit parallel to the portion of structure they are in, and thus be able to rotate. This particular filter does not have the capacity to achieve that yet, but is part of a building block to get there.

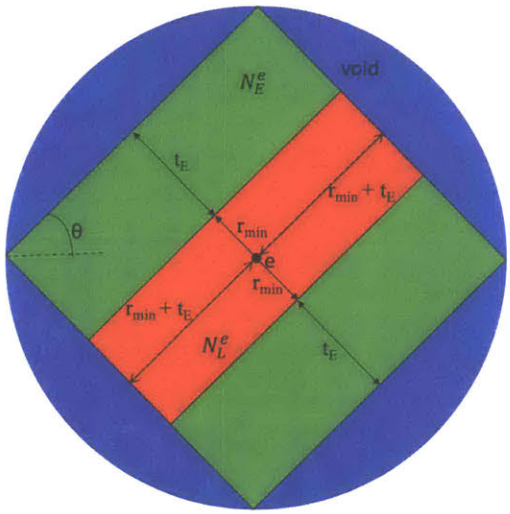

Figure 11. Angled Inclusion Primitive consists of an angled rectangular object (red) of radius r_{min}, an enclosure (green) that controls the minimum object spacing t_E and a void (blue) that is not affected by the element e as in Figure 1

The angled filter interval was determined using the equation of a line. After inspection, the stiff inclusion was determined to be the elements whose vertical distance, from a line drawn from the specific element at a desired angle, θ, was less than or equal to the minimum radius, r_{min_D}, this is expressed by the intervals given in Eq. (27).

$$i \in N_L^e \quad if \begin{cases} |\Delta y - \Delta x * m| \leq \dfrac{r_{min_D}}{\cos\theta} \\ \left|\Delta y + \dfrac{\Delta x}{m}\right| \leq \dfrac{r_{min_D} + t_E}{\cos\theta} \end{cases}$$

$$i \in N_E^e \quad if \begin{cases} \dfrac{r_{min_D}}{\cos\theta} < |\Delta y - \Delta x * m| \leq \dfrac{r_{min_D} + t_E}{\cos\theta} \\ \left|\Delta y + \dfrac{\Delta x}{m}\right| \leq \dfrac{r_{min_D} + t_E}{\cos\theta} \end{cases} \tag{27}$$

where m is the slope of the boundary line of the inclusion calculated as the tan of the angle from positive x-axis.

$$m = \tan\theta$$
$$\Delta x = x_i - \bar{x}^e \tag{28}$$
$$\Delta y = y_i - \bar{y}^e$$

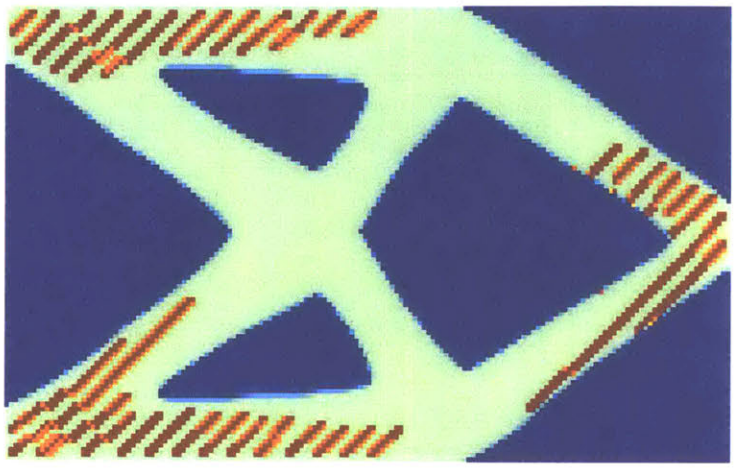

Figure 12. Cantilever Beam with Diagonal Inclusions

Figure 12 shows the 45° inclusions solution for the cantilever design problem. Just as the previous examples, the optimizer places the stiff material around the supports and the load. Here, near the bottom support, it appears the inclusions "walks over" so it goes from the farthest edged into the slanted member. This reaction occurs as a result of the inclusion wanting to fall within the slant. A similar situation occurs on the far end as well. The compliance in this case is 32.49. The solutions for the different examples mentioned are summarized in Table 2.

Table 2. Cantilever Beam Results Summary

Inclusion Shape	V_s (%)	Figure	Compliance
Circular	10	Figure 4	32.76
Circular	7.5	Figure 5	33.76
Horizontal	7.5	Figure 8	29.83
Vertical	7.5	Figure 10	33.16
Diagonal	7.5	Figure 12	32.49

As summarized in Table 2, when the volume constraint on inclusion is decreased, the compliance increases. While comparing the designs using the same volume constraint, it appears the

horizontal inclusion shape provides a much stiffer design by about 12%. Though, the vertical and diagonal designs are only slightly better. This implies that the change in filter shape can be beneficial in design but also provide simpler construction conditions. Though, it also points to some specific orientation of filters being more efficient in specific designs than others. Here, the horizontal inclusion is most efficient.

Simply Supported (MBB) Beam Example

This second test case is an MBB beam with a single gravity load applied on the mid-span. The design domain is shown in Figure 13.

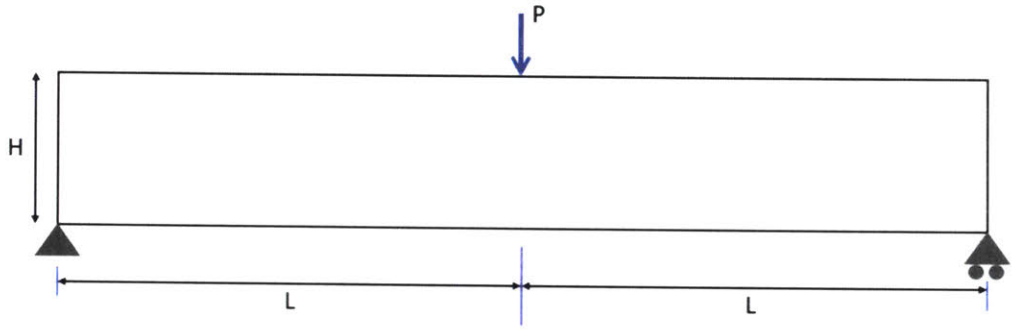

Figure 13. Full MBB Beam Design Domain

To simplify the problem, symmetry is imposed on the beam and it is optimized using the half-beam design domain shown in Figure 14. The half beam length, L, is 60 units, height, H, is 20 units, thickness, t, is 1 unit, and load, P, is 10 units. The finite element mesh used is 240 × 80. The minimum inclusion scale, r_{min_D} is 0.25 units, the minimum distance between objects, t_E, is 0.625 units and the topology length scale, r_{min_T}, is 1.0 unit. The maximum volume of material, V_T, is 40% of V, with a maximum inclusion volume, V_S, of 6% of V. The Poisson's ratio, ν, is 0.3, initial Young's modulus, E, is 100 with material young's modulus factors, E_1 and E_2, at 1 and 3 respectively. The design variable upper bound, φ_{max}, is 1.

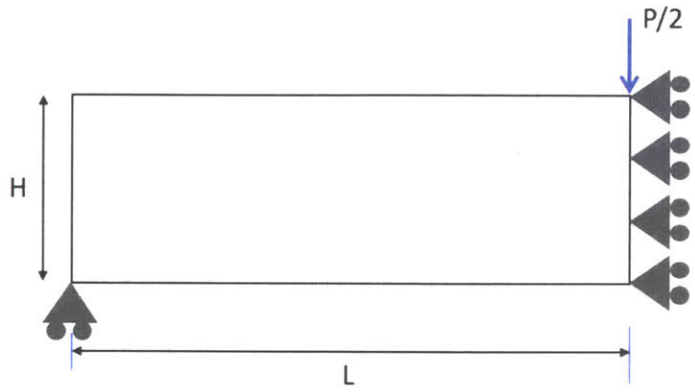

Figure 14. Half MBB Beam Design Domain

The design is performed with all four previously described primitive types; that being circular, horizontal, vertical and diagonal, respectively. The solutions are summarized in Table 3 and shown in Fig. 15-17.

Table 3. MBB Beam Results Summary

Inclusion Shape	Figure	Compliance
Circular	Figure 15	52.88
Horizontal	Figure 16	46.72
Vertical	Figure 17	56.10
Diagonal	Figure 18	54.42

Figure 15. Full MBB Beam with Circular Inclusions

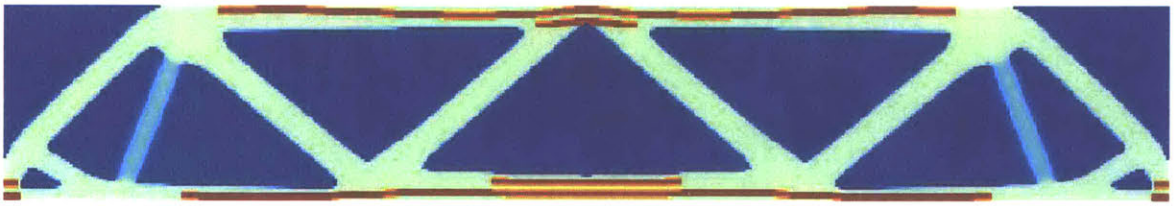

Figure 16. Full MBB Beam with Horizontal Inclusions

Figure 17. Full MBB Beam with Vertical Inclusions

Figure 18. Full MBB Beam with Diagonal Inclusions

In the simply supported beam case, the optimizer places the stiff material mostly in the center at the top and bottom. This is due to the stress distribution of a simply supported beam. It's maximum moment occurs at midspan and therefor its maximum stresses. Here, the horizontal inclusion still proves to be the best solution, this is because it provides the means to apply the most stiff material in the locations the beams need it to be. The portions of the solution that are not as green or blue as the rest occur as a result of the minimum length scale chosen. The rest of the structure has attained the 0-1 binary enforced but due to a combination of the minimum length scale as well as the material volume constraints, those members don't get either fully applied or moved to another region in the design space.

Conclusions

This thesis aimed to develop an algorithm to add complexity to the design completed by Koh and Guest [10]. The algorithm used the combination of HPM and RAMP to obtain multi-material designs using discrete object projection. The discrete objects used where specified stiff circular inclusions surrounded by more compliant material to control minimum object spacing. The algorithm discussed was first reproduced and verified. Then the discrete object filters modified to provide three different object types. The three inclusions used were horizontal filters, vertical filters and diagonal filters. This allows for designs of longitudinal inclusions within some optimized topology. The algorithm was run on the cantilever beam and simply supported beam.

It was discovered that the horizontal inclusions were best for both examples. This is not surprising as this is the form of reinforcing used in practice. A shortcoming of the algorithm is it does not always strictly fulfill the spacing requirement and can require tuning to avoid overlapping objects. This problem gets is more pronounced when the spacing is small compared to the inclusion size and a large inclusion volume is permitted.

For future work, a filter that would allow for the inclusions to slope at varying angles. An implementation of this can be using an additional variable, θ, within the preset inclusion geometry and letting θ dictate which is the local set and which is the enclosure set.

Bibliography

1. Bendsøe MP, Sigmund O. Topology optimization: theory, methods, and applications. Second edition, corrected printing. Berlin Heidelberg: Springer; 2011. 370 p. (Engineering online library).

2. Stromberg LL, Beghini A, Baker WF, Paulino GH. Application of layout and topology optimization using pattern gradation for the conceptual design of buildings. Struct Multidiscip Optim. 2011 Feb;43(2):165–80.

3. Dombernowsky P, Søndergaard A. Three-dimensional topology optimisation in architectural and structural design of concrete structures. 2009;12.

4. Jewett JL, Carstensen JV. Topology-optimized design, construction and experimental evaluation of concrete beams. Autom Constr. 2019 Jun;102:59–67.

5. Ding GKC. Sustainable construction—The role of environmental assessment tools. J Environ Manage. 2008 Feb;86(3):451–64.

6. González MJ, García Navarro J. Assessment of the decrease of CO2 emissions in the construction field through the selection of materials: Practical case study of three houses of low environmental impact. Build Environ. 2006 Jul;41(7):902–9.

7. Wolf CD. Embodied Life Cycle Impacts of Building Structures. :212.

8. Bendsøe MP, Sigmund O. Material interpolation schemes in topology optimization. Arch Appl Mech Ing Arch. 1999 Nov 22;69(9–10):635–54.

9. Gaynor AT, Guest JK, Moen CD. Reinforced Concrete Force Visualization and Design Using Bilinear Truss-Continuum Topology Optimization. J Struct Eng. 2013 Apr;139(4):607–18.

10. Koh S, Guest JK. Topology Optimization of Components with Embedded Objects Using Discrete Object Projection. In: Volume 2B: 43rd Design Automation Conference [Internet]. Cleveland, Ohio, USA: ASME; 2017 [cited 2018 Nov 26]. p. V02BT03A009. Available from: http://proceedings.asmedigitalcollection.asme.org/proceeding.aspx?doi=10.1115/DETC2017-68055

11. Ha S-H, Guest JK. Optimizing inclusion shapes and patterns in periodic materials using Discrete Object Projection. Struct Multidiscip Optim. 2014 Jul;50(1):65–80.

12. Christensen PW, Klarbring A. An introduction to structural optimization. Dordrecht: Springer; 2009. 211 p. (Solid mechanics and its applications).

13. Addis B. Building: 3,000 Years of Design, Engineering, and Construction. Reprint edition. London: Phaidon Press; 2015. 640 p.

14. Zhang XS, Paulino GH, Ramos AS. Multimaterial topology optimization with multiple volume constraints: Combining the ZPR update with a ground-structure algorithm to select a single material per overlapping set: Multimaterial topology optimization with multiple volume constraints. Int J Numer Methods Eng. 2018 Jun 8;114(10):1053–73.

15. Zhang XS, Paulino GH, Ramos AS. Multi-material topology optimization with multiple volume constraints: a general approach applied to ground structures with material nonlinearity. Struct Multidiscip Optim. 2018 Jan;57(1):161–82.

16. Guest JK. Optimizing the layout of discrete objects in structures and materials: A projection-based topology optimization approach. Comput Methods Appl Mech Eng. 2015 Jan;283:330–51.

17. Bendsøe MP. Optimal shape design as a material distribution problem. Struct Optim. 1989 Dec 1;1(4):193–202.

18. Díaz A, Sigmund O. Checkerboard patterns in layout optimization. Struct Optim. 1995 Aug;10(1):40–5.

19. Sigmund O, Maute K. Topology optimization approaches. Struct Multidiscip Optim. 2013 Dec 1;48(6):1031–55.

20. Guest JK, Prévost JH, Belytschko T. Achieving minimum length scale in topology optimization using nodal design variables and projection functions. Int J Numer Methods Eng. 2004;61(2):238–54.

21. Bruns TE, Tortorelli DA. Topology optimization of non-linear elastic structures and compliant mechanisms. Comput Methods Appl Mech Eng. 2001 Mar;190(26–27):3443–59.

22. Bourdin B. Filters in topology optimization. Int J Numer Methods Eng. 2001 Mar 30;50(9):2143–58.

23. Stolpe M, Svanberg K. An alternative interpolation scheme for minimum compliance topology optimization. Struct Multidiscip Optim. 2001 Sep;22(2):116–24.

24. Deaton JD, Grandhi RV. A survey of structural and multidisciplinary continuum topology optimization: post 2000. Struct Multidiscip Optim. 2014 Jan;49(1):1–38.

25. Chandrupatla TR, Belegundu AD. Introduction to finite elements in engineering. [Internet]. 2012 [cited 2019 May 7]. Available from: https://lib.mit.edu/record/cat00916a/mit.002006500

26. Svanberg K. The method of moving asymptotes—a new method for structural optimization. Int J Numer Methods Eng. 1987 Feb;24(2):359–73.